Published in MicroSim II (Simutation and design of microsystems and microstructures), 107-116, 1997 1
which should be used for any reference to this work

Simulation and design of a three axis navigation microsystem based on micromachined sensors

[1]Y. Ansel, [1]Ph. Lerch, [1]Ph. Renaud,[2]F. Paoletti, [2]M.-A. Grétillat, [2]N. F. de Rooij,[3]G. Schröpfer, [3]S. Ballandras,[3]M. de Labachelerie, [2]C. Marselli, [2]H. P. Amann, [2]F. Pellandini
[1]IMS-DMT, EPFL, CH-1015 Lausanne, [2]IMT, University of Neuchâtel, CH-2000 Neuchâtel, [3]LPMO-IMFC, F-25000 Besançon, e-mail: yannick.ansel@ims.dmt.epfl.ch

Abstract

The project presented in this paper aims at defining the limits of microsystems through the realisation of a navigation system based on inertial microsensors. The work includes (i) design, fabrication, characterisation of accelerometers and angular rate sensors, (ii) development of techniques for simulation of sensor behaviour, and (iii) design of a sensor data processing system.

1 Introduction

The advent of microsensors widens the market for navigation systems, limited up to now to costly applications. For example, in automotive applications, microsensors can be used as a complement to GPS navigation (Global Positioning System), especially in urban areas where loss of GPS signals often happens. This application has been chosen in order to evaluate – through the construction of a demonstrator – the limits of today's microsystems.

A navigation system has to compute the position and the orientation relying on the measurements of the accelerometers and angular rate sensors. Unfortunately, microsensors have a non-ideal behaviour, resulting in signal drifts. A suitable data processing has therefore to be designed in order to improve the accuracy of the system. The work has been divided into four parts, which are one by one presented in the paper. A 2D monolithic silicon accelerometer has been designed at LPMO (§2). At IMT, a silicon vibrating angular rate sensor has been realised (§3). At IMS, methods to obtain behavioural models based on finite element techniques are developed (§4). Finally, the data processing based on Kalman filtering, including computation of the navigation parameters and design of an error correction system, is also performed at IMT (§5).

2 2D Monolithic silicon accelerometer

2.1. Principle

For the lateral accelerometer proposed in this section, the displacement of the seismic mass is proportional to the applied acceleration and given by $\Delta x_i = m \cdot k_i^{-1} \cdot a_i$, where Δx_i is the displacement in the i-direction, m the mass, k_i the device's spring constant in the i-direction and a_i the applied acceleration in the i-direction. The spring constants k_i are functions of the geometry of the suspension beams. The presented structure is sensitive only to accelerations in one lateral direction and insensitive to other directions due to the structure's geometry. The mechanical sensitivity of the device is given by the ratio of displacement over acceleration, which is equal, to a good approximation, to the ratio of mass m over spring constant. The static and dynamic behaviour of the device can be computed more precisely with a finite element analysis (§4).

2.2. Fabrication by wet anisotropic etching

Lateral accelerometers have already been fabricated by wet etching of (110) silicon or quartz, surface micromaching, LIGA technique, or by deep plasma etching [1]. In many conventional bulk-micromachined accelerometers, the seismic mass is pyramidal and not symmetrically shaped, leading to large transverse sensitivities. We demonstrate a new fabrication technique for high aspect-ratio flat sidewalls, using anisotropic KOH wet etching of a double sided polished (100) silicon wafer.

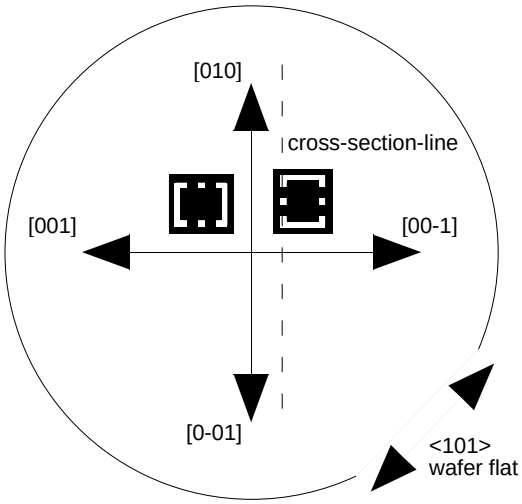

Figure 2.1 : Mask pattern positioned with an angle of 45° from the <110> wafer flat

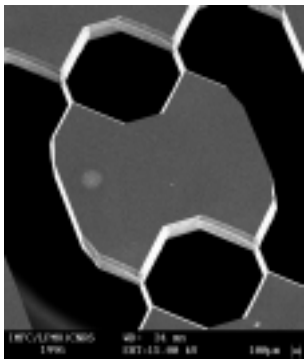

Figure 2.2 : SEM view of the complete symmetrical structure (beam width 11 µm, aspect ratio 35).

On a (100) wafer, it is not possible to achieve vertical sidewalls if the pattern is aligned in the usual direction which is parallel to the <110> wafer flat. Vertical {100} sidewalls are obtained by wet etching in a (100) wafer, with a pattern aligned at ±45° angle from the wafer flat [2] (Figure 2.1). However, this alignment will also result in a large undercut of the mask structure which is equal to the etch depth d. In order to obtain a beam width of w, the width of the mask pattern w_m must therefore be equal to $w_m = w + 2\,d$ (Figure 2.2).

The underetching stop planes are illustrated in figure 2.3. The undercut plane's directions can be identified from the direction of their intersections with the wafer plane. One gets the following design rule for a mask beam length l_m and an effective length l :

$$l_m = l + \frac{t}{\tan(54.74Þ)} + t \approx l + 1707t \qquad (1)$$

where t is the wafer thickness and l the effective length of the fabricated beam. With the fabrication method, one obtains a two-axis accelerometer-system in a single etching step, by simultaneously etching two sensor elements rotated by 90° with respect to each other. Moreover, the 90° angle is precisely defined by the intrinsic crystal orientation. For the third direction, another accelerometer sensing vertical accelerations can be included, resulting in a three-dimensional monolithic seismic mass system, with intrinsic alignment due to the perpendicular {100} crystal planes.

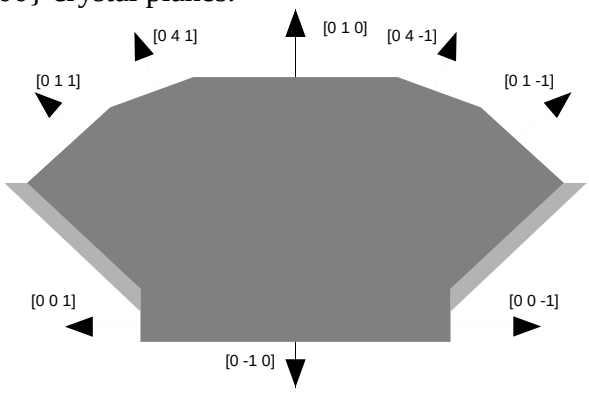

Figure 2.3 : Half view of the structure with indexed undercut directions

2.3 Detection techniques

A possible on-chip detection technique makes use of a capacitive transducer. The change of the capacitance between comb-shaped electrodes placed on the movable seismic mass and a fixed counterpart on an anodic bonded substrate is proportional to the lateral displacement [3].

Another possibility is a fibre optic interrogation [4]. An optical fibre can be easily attached in front of the movable seismic mass to form a low finesse interferometer. The vertical sidewalls of the seismic mass consist of (100) crystal silicon planes which enable good light reflection. The optical fibre links the device to an optoelectronic detection unit. The system possesses all the advantages of passive interferometric methods, like immunity to electro-magnetic interference, high sensitivity, possible operation in hazardous environment, and optical multiplexing of many sensors on a single fibre.

3 Silicon angular rate sensor

Low cost silicon micromachined gyroscopes (angular rate sensors) are promising devices for navigation platforms. Different types have been reported [5-9] which use either piezoelectric [5], electrostatic [6-8] or electro-magnetic [9] actuation and piezoelectric [5] or capacitive [6-9] detection.

3.1 Principle

This new gyroscope is based on the tuning fork principle [10,11]. As shown in figure 3.1, it is operated by vibrating two tines antiphase in one plane and measuring the effect of the Coriolis force in the orthogonal plane. The tines are constructed from two proof masses suspended by four beams. Figure 3.2 illustrates the excitation principle of this sensor as well as its detection principle. A constant magnetic field (B) is provided by a magnet placed on top

of the device (Figure 3.3). When an AC current flows along the metallic conductor placed on top of the proof masses, the U-shaped design of this line results in an antiphase Lorentz force. The vertical movement of the proof masses due to the Coriolis force is sensed by four p-type piezoresistors centred on top of the external suspensions and connected in a Wheatstone bridge configuration.

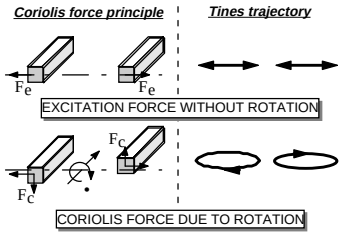

Figure 3.1 : Principle of the tuning fork vibratory gyroscope

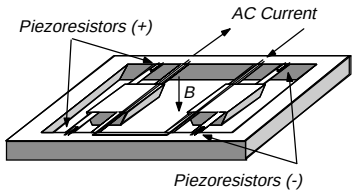

Figure 3.2 : Gyroscope with electromagnetic excitation and piezoresistive detection

3.2 Fabrication technology

Double side polished n-type silicon wafers are used for the fabrication of the gyroscopes. The first processing steps concern the top side of the wafer. The four boron doped piezoresistors are implanted. A metallic layer is deposited and patterned to build the excitation line and to interconnect the piezoresistors.

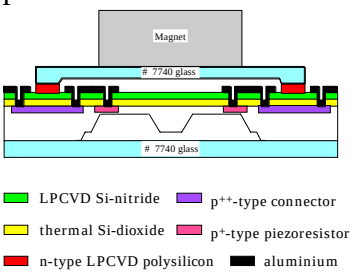

Figure 3.3 : Cross section along the external beams and the proof mass

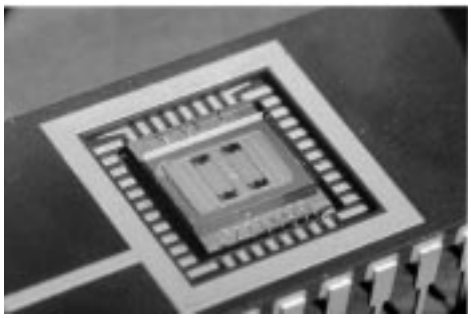

Figure 3.4 : Packaged prototype, before assembling of the magnet (proof masses 2 x 1 x 0.36 mm^3)

A silicon nitride passivation layer is deposited on top of the structure and opened to access the bonding pads. Then the proof masses are structured from the back side in KOH etching, while the top side of the wafer is protected with a chuck. Finally the beams are structured by plasma etching. Beams with well defined sidewalls can be fabricated. A good control of the beam's dimension leads to a better mechanical behaviour of the proof masses. Before chip dicing, anodic bonding of two glass wafers is performed to encapsulate the silicon sensing elements (Figure 3.3). The top glass plate has been micromachined to define a cavity that ensures an overrange protection of the masses (Figure 3.4).

3.3 Test results

The output signal of the sensor has been amplified and filtered by a lock-in amplifier. Figure 3.5 shows the frequency response caused by the electro-

magnetic excitation without rotation. This measurement clearly demonstrates the good matching of the resonance frequencies of the two proof masses. The superposition of the individual signals gives a single amplitude peak and a phase change of 360°.

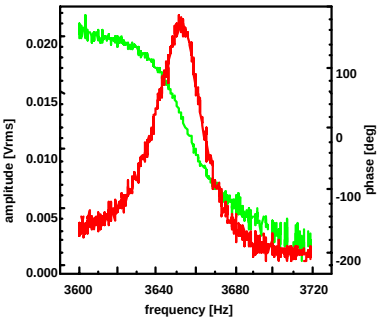

Figure 3.5 : Frequency response of the prototype gyroscope (proof masses 2 x 1 x 0.36 mm^3)

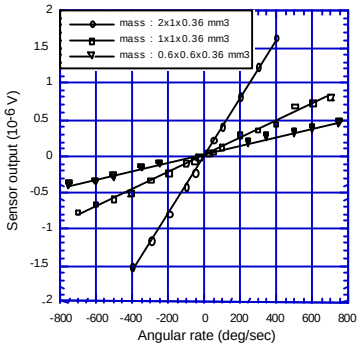

Figure 3.6 : Output signal of 3 prototype gyroscopes at different angular rates (excitation current AC : 4.5 mA)

First characterisation of the gyroscope on a rotating table shows extremely promising results. Several angular rotation rates ranging from -750 deg/s to 750 deg/s have been applied to different prototype gyroscopes. The three curves presented in Figure 3.6 illustrate that the sensitivity of the sensors increases with the size of the proof masses, which points out the possibility of covering different ranges by an appropriate scaling of the sensor. The three prototypes show excellent linearity: a non-linearity between 0.04 % and 0.19 % has been observed, while a 4 nV/deg/s sensitivity has been obtained with the largest mass.

4 Mechanical modelling and simulation of inertial sensors

Simulation of the device properties in the design phase allows to compare different prototype designs and then to reduce the development cost. In order to optimise designs of navigation systems, the mechanical sensitivities of accelerometers and vibrating gyroscopes are evaluated by simulation.

4.1 Evaluation of the inertial sensor's sensitivity

In order to evaluate gyroscopic sensitivities of angular rate sensors, an iterative simulation procedure has been proposed [12]. To determine sensitivity, the following equation describing the linear dynamic behaviour of a rotating structure has to be solved :

$$[M]\frac{d^2\mathbf{u}}{dt^2}+[G]\frac{d\mathbf{u}}{dt}+[C]\frac{d\mathbf{u}}{dt}+[K]\mathbf{u}=\mathbf{F}_e \qquad (2)$$

[M] is the mass matrix of the structure, [C] the damping matrix, [K] the stiffness matrix, **u** the displacement vector, $\mathbf{F}_e$ the excitation forces and [G] the gyroscopic coupling matrix, depending on the rotation speed. Equation 2 is solved numerically using the following iterative process. First, the harmonic response **u** of the system, without rotation, is computed using finite element harmonic (FE) analysis.

Figure 4.1 : Iterative process for angular rate sensitivity computation

Next, the gyroscopic solution **u** is computed on the base of the previous results taking into account Coriolis forces. Again, the algorithm shown above is used. Here, Coriolis forces are added to other loads in a second step. Usually, n = 2 leads directly to a converged solution with a small error when the rotation speed is low with respect to the excitation frequency. Comparing results for pure harmonic and gyroscopic analysis, the mechanical sensitivity of an angular rate sensor is calculated. The method has been applied to a FE model of the gyroscope (§ 3), and simulation results are consistent with measurements [12,14]. In order to determine the sensitivity of the accelerometer, a static analysis was performed on a FE model of the accelerometer (§ 2). Constant acceleration was applied to the structure and the mechanical sensitivity deduced.

4.2 Behavioural modelling based on finite element models

The assembly of low-power devices in a confined space results in strong coupling of physical quantities between the components of a microsystem. In the design phase, this implies that in addition to individual component simulation, a global system simulation has to be performed to adequately predict system performance, possibly including electronic devices.

Behavioural models for the ELDO™ simulator – written in HDL-A™, a hardware description language used in analogue electronics – are therefore generated from FE simulations performed on the ANSYS™ FE software using the parameter extractor tool pxt [13,15]. For the generation of linear dynamic models, an automatic process has been developed.

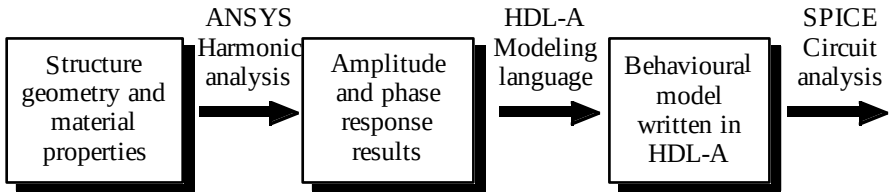

Figure 4.2 : Behavioural modeling flow process

Classical FEM harmonic analysis is performed on ANSYS™. Next, data files are created that contain real and imaginary device response values of a physical quantity of interest (displacement, stress, etc.) as a function of frequency, i.e. the discrete frequency response (amplitude and phase). Finally, behavioural models in HDL-A to be used on SPICE like simulators are generated using a polynomial filter approach.

Those models derived from harmonic FEM analyses are valid for DC, AC and transient SPICE analysis domains. The HDL-A model can be used with standard network analysis files, the simulation results being stored in a wave form database. Note that the data files can also be created from results of tests performed on experimental devices.

Figure 5.1 : Inertial Process

The main part of the algorithm is the computation of the transformation matrix between the measurement frame (vehicle frame) and the computation frame (earth-fixed frame). To reduce computational load and to avoid loss of accuracy by using trigonometric functions, quaternions are used [16, 19].

5.2 Discrete Kalman Filtering

Several reasons make the Kalman filter (e.g. [17]) a tool rather often used for navigation applications. The algorithm is formed of a set of recursive formulae and is suitable for real time processing. It requires a system description convenient for multi input/output configurations. A Kalman filter is an optimal

Figure 5.2 : Kalman filter design

5.3 Test set-up and results

We worked mainly with off-the-shelf sensors before using the presented inertial sensors (§2 and §3). The accelerometer ADXL05 (Analog Devices) is a low-cost surface-micromachined uniaxial sensor with capacitive detection. The full scale can be fixed from ±1 g to ±5 g, the sensitivity from 200mV/g to 1 V/g. The Gyrostar ENC-05S (Murata) is a small and relatively inexpensive vibrating piezoelectric gyro. The maximum rate that can be measured is 90 deg/s, the sensitivity is 0.008 mV/deg. Processing algorithms are developed using Matlab™ and are implemented on Texas Instruments TMS320C32 digital signal processor (DSP). For test purposes, we use as a demonstrator a scale train carrying the microsensors (Figure 5.4). Absolute references are provided by optical sensors put along the tracks.

As an illustration, an example of a model for the gyro (§2) offset variation is given (Figure 5.3). The chosen model is a combination of two random processes: the main variation is modelled by a random-walk to which a coloured noise (order 2 auto regressive model) is added. Improvements of the gyroscope stability is expected by integrating this model in the Kalman filter. Experiments show the ability of the system to deliver corrected results. Figure 5.5 shows the effect of correction for an measured 8-shaped scale train trajectory, realised with the second Kalman filter.

Figure 5.5 : Train trajectory without (left) and with (right) correction. The thick 8-shaped curve stands for the true trajectory

6 Conclusion

In this paper, the design of a three axis navigation microsystem was presented in four parts : the accelerometer, the angular rate sensor, simulation, and data processing. The 2D monolithic accelerometer consists of two perpendicular silicon masses. Detection relies on capacitive or optical methods. The gyroscope consists of two proof masses, electromagnetically excited in antiphase. The perpendicular movement due to Coriolis forces is measured by four piezoresistors connected in a Wheatstone bridge configuration. FE mechanical simulation of inertial sensors leads to behavioural models – written in the hardware description language HDL-A and therefore compatible with the processing electronics. Finally, data processing is developed using a Kalman filtering algorithm. It includes computation of navigation parameters as well as error correction. Each part of the inertial platform will be improved in order to optimise the system's performance. Further tests are planned (e.g. in a running car) to determine the technical limits.

7 Acknowledgements

This work has been funded by the Swiss National Science Foundation (FNSRS), the Swiss Foundation for Research in Microtechnology (FSRM) and the French National Centre for Scientific Research (CNRS) in the frame of an exchange between French and Swiss institutions active in the field of microtechnology.

Index

navigation microsystem, microaccelerometer, microgyroscope, Kalman, HDL-A

References

[1] G. Delapierre, “Microtechnology: limits and opportunities through the example of accelerometers”, Proc. Eurosensors'96, Leuven, Belgium, 1083-1092

[2] G. Schröpfer, S. Ballandras, M. de Labachelerie, P. Blind, Y. Ansel, “Fabrication of a new highly symmetrical, in-plane accelerometer-structure by anisotropic etching of (100) silicon”, to be published in Journal of Micromechanics and Microengineering (1997)

[3] Y. Ansel, B. Romanowicz, Ph. Renaud, G. Schröpfer, “Optimisation of a linear capacitive transducer for a silicon accelerometer by finite element simulation”, submitted to EUROSENSORS XI, Warshaw, Poland, Sept. 21-24, 1997

[4] G. Schröpfer, W. Elflein, M. de Labachelerie, H. Porte, S. Ballandras, “(100) silicon in-plane microaccelerometer with remote optical read-out based on coherence modulation”, submitted to EUROSENSORS XI, Warshaw, Poland, September 21-24, 1997

[5] J. Söderkvist, "Design of a solid-state gyroscopic sensor made of quartz", Sensors and Actuators, A21-A23, (1990), pp. 293-296

[6] P. Greiff, "Silicon monolithic gyroscope", Techn. Dig. Transducers '91, San Fransisco, CA, (1991), pp. 966-968

[7] J. Bernstein, "A micromachined comb-drive tuning fork rate gyroscope", Proc. IEEE MEMS Workshop '93, Fort Lauderdale, Florida (1993), pp. 143-148

[8] M.W. Putty, "A micromachined vibrating ring gyroscope", Proc. IEEE Solid State Sensor and Actuator Workshop '94, Hilton Head, South Carolina (1994), pp. 213-220

[9] M. Hashimoto, "Silicon resonant angular rate sensor using electromagnetic excitation and capacitive detection", Proc. Micro System Technologies '94, Berlin, Germany (1994), pp. 763-771

[10] F. Paoletti, M. A. Grétillat, N. F de Rooij, “A silicon vibrating gyroscope with piezoresistive detection and electromagnetic excitation”, Proc. IEEE MEMS Workshop’96, San Diego, CA (1996), pp. 162-167

[11] F. Paoletti, M.-A. Grétillat, N. F de Rooij, “A silicon micromachined tuning fork gyroscope”, Proc. Symposium Gyro Technology, Stuttgart, Germany (1996), pp. 5.0-5.8

[12] Y. Ansel, B. Romanowicz, Ph. Lerch, Ph. Renaud, "Optimisation of a vibrating gyroscope by system level simulation." Proc. of Eurosensor X, Leuven (B), Sept 8-11 1996, Vol. 4 , pp. 1245-1248

[13] B. Romanowicz, Y. Ansel, Ph. Lerch, Ph. Renaud, "Global modeling and simulation of microsystems", Proc. MME'96 Micromechanics Europe, Barcelona (E), Oct. 21-22 1996, pp. 196-199

[14] Y. Ansel, Ph. Lerch, Ph. Renaud, "Mode coupling aspects in a vibrating gyroscope." to be published in Sensors and Actuators : A. Physical

[15] B. Romanowicz, A. Vachoux, Y. Ansel, M. Laudon, C. Amacker, Ph. Renaud, G Schröpfer, “VHDL-1076.1 Modeling examples for microsystem simulation”, Proc. 2nd Workshop on Librairies, Component Modelling and Quality Assurance accompanying CHDL Symposium 97, Toledo (E), 1997

[16] Grubin C., "Derivation of the quaternion scheme via the Euler axis and angle", Engineering Notes, Journal of Spacecraft, 1970, Vol. 7, n°10, pp. 1261-1263

[17] Brown R. G., Hwang P. Y. C., "Introduction to random signals and applied Kalman filtering", 2nd edition, John Wiley & Sons, Inc., New York, 1992

[18] Ljung L., "System identification - Theory for the user", Prentice Hall, 1987

[19] C. Marselli, H. P. Amann, F. Pellandini, "Error correction applied to microsensors in a navigation application", Proc. Mecatronics, Besançon (F), 1996, Vol. 2, pp. 650-655